2013

A Single-Switch LCL-Resonant Isolated DC-DC Converter

Jianwu Zeng
University of Nebraska-Lincoln, jzeng@huskers.unl.edu

Wei Qiao
University of Nebraska–Lincoln, wqiao@engr.unl.edu

Liyan Qu
University of Nebraska-Lincoln, lqu2@unl.edu

Energy Conversion Congress and Exposition (ECCE), 2013 IEEE
Year: 2013
Pages: 5496 - 5502, DOI: 10.1109/ECCE.2013.6647447

A Single-Switch LCL-Resonant Isolated DC-DC Converter

Jianwu Zeng, Wei Qiao*, and Liyan Qu
Power and Energy Systems Laboratory
Department of Electrical Engineering
University of Nebraska-Lincoln
Lincoln, NE, 68588-0511 USA
jzeng@huskers.unl.edu; wqiao@engr.unl.edu; lqu2@unl.edu

***Abstract*—Isolated converters are desirable in the DC-DC power conversion applications where isolation and/or a large voltage step-up gain is needed. Traditional isolated DC-DC converters either utilize many switches to achieve high efficiency or use few switches which result in low efficiency. This paper proposes a new single-switch isolated DC-DC converter with a LCL-resonant circuit. The proposed isolated DC-DC converter has the advantages of not only using the least number of (i.e., one) switch, but also achieving zero-current switching (ZCS) and zero-voltage switching (ZVS) when the switch is turned on and off, respectively. Experimental results are provided to validate the theoretical analysis and simulation. The proposed converter has achieved the maximum efficiency of 93.5%, which is higher than the corresponding hard-switching converter with a similar topology.**

***Index Terms*—Isolated DC-DC converter, LCL resonance, single-switch converter, soft switching.**

I. INTRODUCTION

In the systems such as batteries and photovoltaic systems where the output voltages of the sources are low, step-up DC-DC converters are commonly used to regulate the voltages to the desired higher values. This type of converters acts as a "DC transformer" to convert the lower-level voltage to a higher-level voltage required by a subsequent converter.

Many topologies have been proposed for step-up DC-DC converters, which in general can be classified into two categories: isolated topologies and nonisolated topologies [1]. Nonisolated converters include various boost type converters [2]-[5]. Their voltage ratios can be further increased by using the cascaded [6] or coupled-inductor [7] technique. In the applications where the step-up voltage regulation ratios are not high, the nonisolated converters usually have higher efficiency than the isolated topologies because no galvanic transformers are used.

On the contrary, in the applications that require high voltage regulation ratios, the isolated topologies are preferable, since they can achieve higher efficiency than nonisolated converters by properly designing the transformer's turn ratio to get the optimal duty cycle. Moreover, an isolated converter provides isolation between the input and output, which is desired from the safety perspective.

A number of isolated converters have been proposed for power factor correction [8]-[9] and high voltage step-up applications [10]-[11]. These topologies include push-pull, isolated boost [8], isolated inductor-fed boost [10]-[11], and isolated buck-boost topologies [12]. Some of them have certain limitations. For example, the duty cycle of the converter in [9] should be set larger than 50% even in the start-up mode. The inductor-fed boost converter in [10] has a high voltage stress across the switch when it is turned off, and an additional voltage clamp circuit is required. Moreover, the aforementioned converters use either four or two switches for each source. Therefore, they have higher hardware costs and more complicated topologies compared with the forward/flyback converter which requires only one switch.

Recently, the authors proposed a new isolated boost converter only using one switch [15]. The converter is capable of delivering power during the whole switching period and has a smaller transformer than that in the forward/flyback converter. However, it has a high voltage stress when the switch is turned off due to the hard switching. To overcome this disadvantage, a soft-switching circuit is introduced in the converter in this work.

The soft switching technique has been implemented for the single-switch converters using a resonant circuit, which consists of the transformer leakage inductance and the added capacitance [16]-[18]. Then the zero-voltage switching (ZVS) can be achieved in the switch, while the rectifier diodes on the secondary side of the transformer are turned on under the zero-current switching (ZCS) condition [17]. Meanwhile, the efficiency of the converter was increased owing to the soft switching.

This paper presents a new single-switch, LCL-resonant, isolated, DC-DC converter. It not only benefits from the merits of soft switching by reducing the voltage stress across the switch, but also increases the efficiency of the converter. The proposed DC-DC converter can be easily

This material is based upon work supported by the Federal Highway Administration under Agreement No. DTFH61-10-H-00003. Any opinions, findings, and conclusions or recommendations expressed in this publication are those of the authors and do not necessarily reflect the view of the Federal Highway Administration.

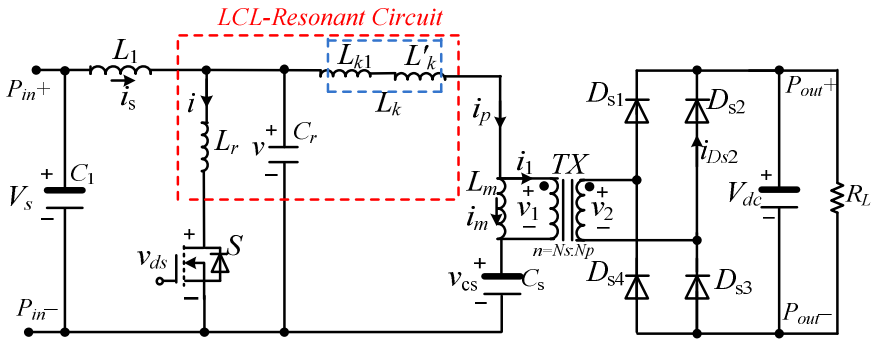

Fig. 1. Proposed single-switch, LCL-resonant, isolated, DC-DC converter.

extended to a multiport converter [19] for integrating multiple sources.

II. Topology And Operating Principle of the Proposed Converter

The circuit diagram of the proposed converter is shown in Fig. 1, which consists of a high-frequency transformer, a switch S, an energy storage capacitor C_S, a full-bridge rectifier, and a LCL-resonant circuit, which consists of two inductors L_r and L_k and a capacitor C_r, where L_k includes the introduced inductance L_{k1} and the leakage inductance of the transformer L'_k. To simplify the analysis, several assumptions are made.

1) The transformer is modeled as a leakage inductance L'_k, a magnetizing inductance L_m with an ideal transformer. Its turn ratio is defined as: $n = N_s / N_p$, where N_s and N_p represent the numbers of turns of the primary and secondary windings, respectively.

2) The body diode of the switch is ideal, i.e., the forward voltage of the diode is zero.

3) The capacitances C_1, C_s, and C are sufficiently large so that their steady-state voltages are constant.

In the steady state, $V_{Cs} = V_s$, where V_s is the converter input voltage. The converter has seven operating modes depending on the states of the switch and the resonant circuit. The differential equations of the resonant circuit in Mode k (k = 1, ⋯, 7) are

$$\begin{cases} v = L_r^{(k)} \cdot \dfrac{di_r^{(k)}}{dt} \\ i_s = C_r \cdot \dfrac{dv}{dt} + i_r^{(k)} \end{cases} \tag{1}$$

where v represents the voltage of the capacitor C_r; $L_r^{(k)}$ and $i_r^{(k)}$ represent the equivalent resonant inductance and the current flowing through the equivalent resonant inductor in the k^{th} (k = 1, ⋯, 7) operating mode, respectively. Then v can be solved from (1) and has the following form.

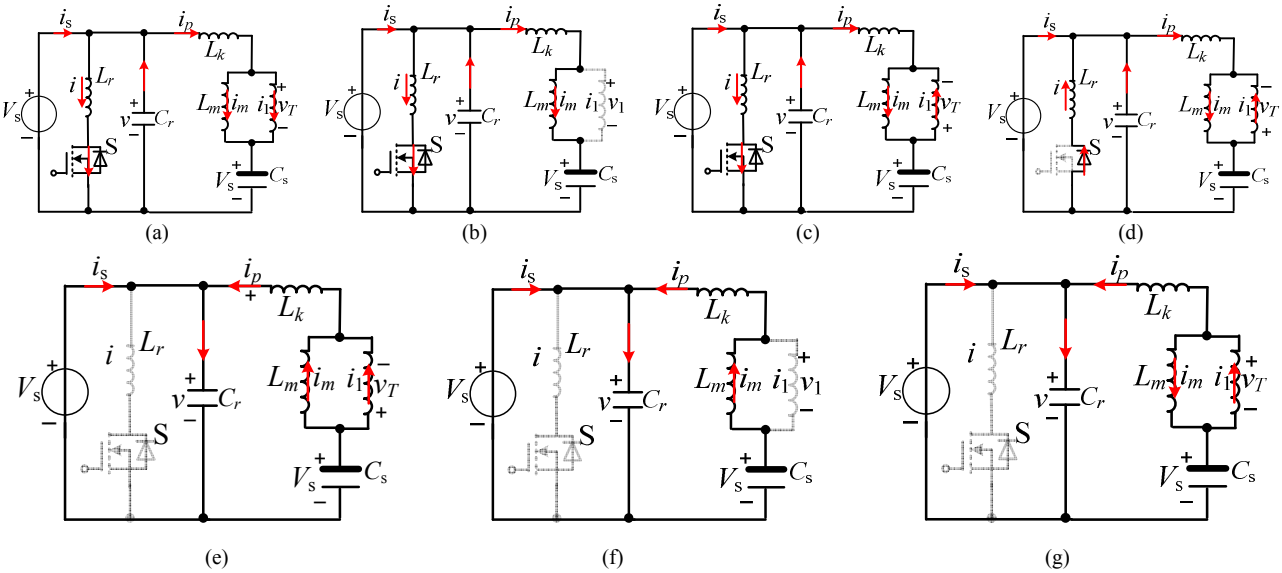

Fig. 2. Equivalent circuits for different operating modes. (a) Mode 1: S is on, $i > 0$, $i_1 > 0$, $v_1 = V_T$; (b) Mode 2: S is on, $i > 0$, $i_1 = 0$; (c) Mode 3: S is on, $i > 0$, $i_1 < 0$, $v_1 = -V_T$; (d) Mode 4: S is being turned off, $i < 0$, $v_1 = -V_T$; (e) Mode 5: S is off, $i = 0$, $v_1 = -V_T$; (f) Mode 6: S is off, $i = 0$, $i_1 = 0$; (f) Mode 7: S is off, $i = 0$, $v_1 = V_T$.

$$v(t) = A_k \cos\left(\omega_k \left(t - t_k\right)\right) + B_k \sin\left(\omega_k \left(t - t_k\right)\right) + V_k^* \quad (2)$$

where ω_k is the resonant frequency in Mode k, V_k^* is the special solution of $v(t)$ in Mode k (k = 1, ⋯, 7), and A_k and B_k are coefficients, which can be expressed as:

$$A_k = v(t_k) - V_k^*, B_k = \frac{I_s - i_p(t_k) - i(t_k)}{\omega_k \cdot C_r} \quad (3)$$

where $v(t_k)$, I_s, $i_p(t_k)$, and $i(t_k)$ represent the voltage of C_r, and the currents of L_1 (i_s can be viewed as a constant value I_s because of a large L_1), L_k, and L_r at time t_k, respectively. Equation (3) indicates that only ω_k and V_k^* are required to determine the coefficients of (2).

The equivalent circuits and steady-state waveforms of the seven operating modes of the converter are shown in Figs. 2 and 3, respectively. To facilitate the explanation of the converter operation, define $V_T = V_{dc}/n$ the equivalent output voltage of the converter referred to the primary side of the transformer.

Mode 1: $t \in [t_1, t_2]$ (see Fig. 3). Prior to Mode 1, the switch S is off, and the current flowing through L_r and L_k are zero and a positive value I_s, respectively, i.e., $i(t_1) = 0$, $i_p(t_1) = I_s$. When S is on, as shown in Fig. 2(a), L_r and L_k resonate with C_r; the current of the inductor L_r increases and the voltage of the capacitor C_r decreases. Due to the existence of L_r, the current of the switch increases slowly so that the switch is turned on under the ZCS condition. The circuit equations in this mode can be expressed as:

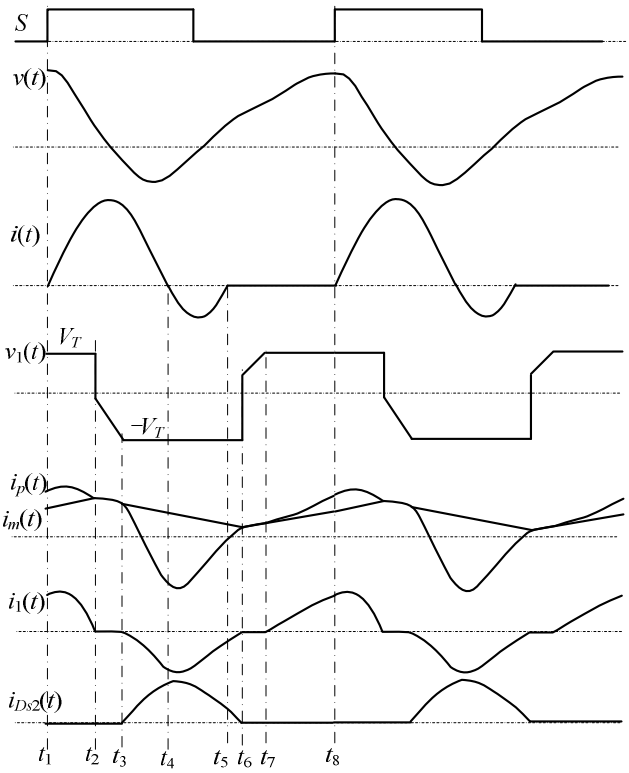

Fig. 3. Steady-state waveforms of the proposed converter.

$$\begin{cases} L_r \cdot \dot{i} = v \\ C_r \cdot \dot{v} = -i - i_p + i_s \\ L_k \cdot \dot{i}_p = v - V_s - V_T \\ L_m \cdot \dot{i}_m(t) = V_T \end{cases} \quad (4)$$

Then

$$\omega_1 = 1/\sqrt{\left(L_r \,//\, L_k\right) \cdot C_r} \quad (5)$$

$$V_1^* = \frac{L_r}{L_r + L_k} \cdot \left(V_s + V_T\right) \quad (6)$$

where // represents that L_r and L_k are connected in parallel; i_m is the current flowing through the primary magnetizing inductor L_m. At the end of Mode 1, $i_p(t_2) = i_m(t_2)$, $i_1(t_2) = 0$, and $v_1(t)$ changes its polarity from positive to negative .

Mode 2: $t \in [t_2, t_3]$, during which S is on, $i_p(t) = i_m(t)$, and $i_1(t) = 0$. As shown in Fig. 2(b), the primary magnetizing inductance L_m, L_k, and L_r resonate with C_r. The equations in this mode can be described as follows:

$$\begin{cases} L_r \cdot \dot{i} = v \\ C_r \cdot \dot{v} = -i - i_p + i_s \\ \left(L_m + L_k\right) \cdot \dot{i}_p = v - V_s \end{cases} \quad (7)$$

Since $L_m >> L_k$, $L_m >> L_r$, then

$$\omega_2 = 1/\sqrt{\left[L_r \,//\, (L_k + L_m)\right] \cdot C_r} \approx 1/\sqrt{L_r \cdot C_r} \quad (8)$$

$$V_2^* = \frac{L_r}{L_r + L_k + L_m} \cdot V_s \approx \frac{L_r}{L_m} \cdot V_s \quad (9)$$

At the end of Mode 2, $v_1(t_3) = -V_T$.

Mode 3: $t \in [t_3, t_4]$, during which S is on, $i(t) > 0$, $v_1(t) = -V_T$, $i_{Ds2}(t) > 0$; as shown in Fig. 2(c), L_r and L_k resonate with C_r; the energy stored in L_r is released to charge the capacitor C_r; v_1 is clamped to $-V_T$. The equations can be expressed as follows.

$$\begin{cases} L_r \cdot \dot{i} = v \\ C_r \cdot \dot{v} = -i - i_p + i_s \\ L_k \cdot \dot{i}_p = v - V_s + V_T \\ L_m \cdot \dot{i}_m = -V_T \end{cases} \quad (10)$$

Then $\omega_3 = \omega_1$,

$$V_3^* = \frac{L_r}{L_r + L_k} \cdot \left(V_s - V_T\right) \quad (11)$$

Mode 4: $t \in [t_4, t_5]$, during which S is on, as shown in Fig. 2(d), the negative current flows through the internal diode of the switch, then the switch can be turned off at any time in this mode under the ZVS condition. The equations are the same as those in Mode 3. Then $\omega_4 = \omega_3$, $V_4^* = V_3^*$.

At the end of this mode, $i(t_4) = 0$ and S is fully turned off.

Mode 5: $t \in [t_5, t_6]$, during which S is off, $i(t) = 0$, $i_1(t) < 0$, $v_1(t) = -V_T$. As shown in Fig. 2(e), L_r and the switch S can be neglected in the circuit. The inductor L_k resonates with the capacitor C_r. The equations are expressed as:

$$\begin{cases} C_r \cdot \dot{v} = -i_p + i_s \\ L_k \cdot \dot{i}_p = v - V_s + V_T \end{cases} \quad (12)$$

Then

$$\omega_5 = 1/\sqrt{L_k \cdot C_r} \quad (13)$$

$$V_5^* = V_s - V_T \quad (14)$$

At the end of Mode 5, $i_{Ds2}(t_6) = 0$, $v_1(t)$ changes its polarity from negative to positive.

Mode 6: $t \in [t_6, t_7]$, during which S is off, $i_p(t) = i_m(t)$ and $i_1(t) = 0$. As shown in Fig. 2(f), L_m and L_k resonate with C_r, and C_r is charged in this mode.

$$\begin{cases} C_r \cdot \dot{v} = -i_p + i_s \\ (L_k + L_m) \cdot \dot{i}_p = v - V_1 \end{cases} \quad (15)$$

Then $V_6^* = V_s$,

$$\omega_6 = 1/\sqrt{(L_k + L_m) \cdot C_r} \quad (16)$$

At the end of Mode 6, $v_1(t_7) = V_T$.

Mode 7: $t \in [t_7, t_8]$, during which S is off, $i_1(t) > 0$, $v_1(t) = V_T$. As shown in Fig. 2(g), L_k resonates with C_r, and

$$\begin{cases} C_r \cdot \dot{v} = -i_p + i_s \\ L_k \cdot \dot{i}_p = v - V_s - V_T \end{cases} \quad (17)$$

Then $\omega_7 = \omega_5$, $V_7^* = V_s + V_T$.

Once S is turned on at time t_8, Mode 7 switches to Mode 1.

III. Components Design

Given the input voltage V_s, power P, and the load resistance R_L, the input current I_s, transformer's turn ratio n, and output voltage V_{dc} can be calculated. The quality factor of this LCL-resonant converter can be calculated as:

$$Q = \frac{R_{ac}}{Z} \quad (18)$$

$$R_{ac} = \frac{8 \cdot R_L}{n^2 \cdot \pi^2} \quad (19)$$

where R_{ac} is the equivalent resistance [20] of the load resistance referred to the primary side of transformer, and Z is the characteristic impedance of the resonant circuit which is defined below.

$$Z = \sqrt{\frac{L_r \,//\, L_k}{C_r}} \quad (20)$$

Z can be calculated from (18) and (19) if the desired Q and R_L are given. Then C_r can be calculated from (5) and (20) by given the resonant frequency. After C_r is determined, $L_r \,//\, L_k$ can be calculated from (20).

The capacitance C_s can be determined as follows [15]:

$$C_S = \frac{P \cdot D \cdot T}{V_T \cdot \Delta v_{cs}} \quad (21)$$

where T is the switching period; D is the duty cycle; Δv_{cs} is the predefined voltage ripple of the capacitor C_s.

The maximum current ($I_{\max}$) flowing through the switch is achieved at time t_p when $v = 0$, then

$$I_{\max} = \frac{v(t_1) - V_1^*}{\omega_1 \cdot L_r} \sin(\omega_1 \cdot t_p) + \frac{V_1^*}{L_r} \cdot t_p \quad (22)$$

where

$$t_p = \cos^{-1}\left(\frac{-V_1^*}{v(t_1) - V_1^*}\right) \quad (23)$$

Then the switch is selected according to the maximum current calculated by (22) and the peak voltage $v(t_1)$ of the capacitor C_r.

IV. Simulation Results

Simulation studies are carried out in MATLAB/Simulink to validate the proposed converter. The switching frequency is 80 kHz; the nominal input voltage is 15V; the load R_L = 50Ω; the transformer turn ratio is n = 14:6; Q is set 4.5 in this paper; and the inductance and capacitance values are listed in Table 1.

Table 1: Inductance and capacitance.

Inductance (μH)				Capacitance (μF)	
L_r	3.3	L_k	3.5	C_r	0.59
L_m	85	L_1	560	C_1, C_s, C	1000

Fig. 4 shows the simulated steady-state waveforms, which well replicate the theoretical waveforms shown in Fig.

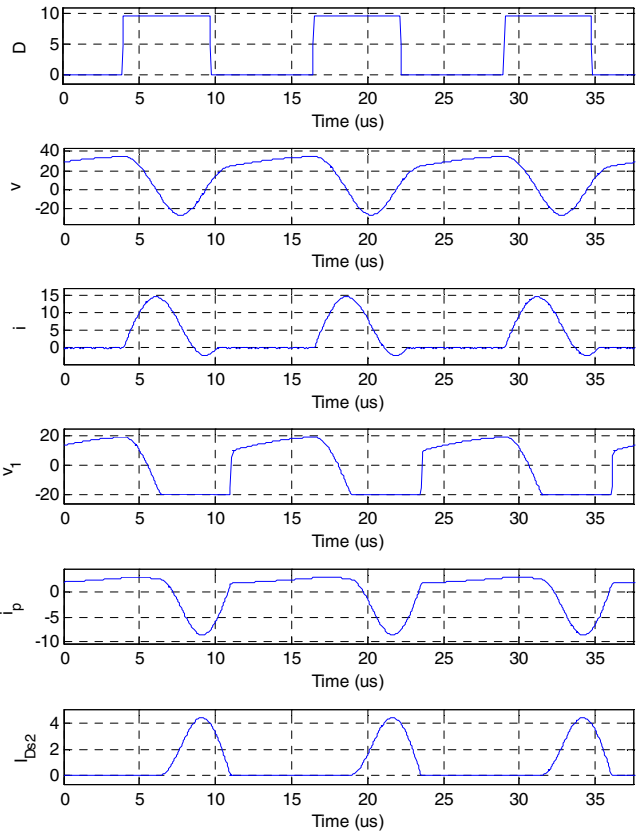

Fig. 4. Steady-state waveforms of the proposed converter.

3. As shown in Fig. 4, when the switch is on, the cosine waveform of the voltage v across C_r and the sine waveform of i indicate the resonance between C_r and L_r. When the current flowing through switch changes its direction from a positive value to a negative value, it indicates that the body diode of the switch is conducted, then the switch can be turned off under the ZVS condition.

V. Experimental Results

To further verify the simulation results, a 100-W prototype of the proposed converter is constructed. The experimental setup is shown in Fig. 5, it consists of the proposed converter where the LCL-resonant components are highlighted, an eZdsp F2812 control board, and a resistive load R_L. A low on-resistance (10.7 mΩ) MOSFET (IPB107N3) is used as the switch of the converter, the rectifier diodes D_{s1}~D_{s4} are selected be EGP50D-E3/54. Other parameters are set the same as those used in the simulation studies.

Fig. 7 shows the voltage (v_{ds}, CH2) and current (i, CH3) waveforms of the switch. When the switch is turned on, the current flowing through the switch increases slowly such that the switch is turned on under the ZCS condition. When the direction of the current flowing through the switch reverses, the switch is turned off under the ZVS condition. After the switch is turned off, the current flowing through the switch drops to zero from a negative value; a high-frequency (approximately 3 MHz) resonance occurs between L_r and the parasitic capacitance of the switch, which results in the oscillation of the switch voltage.

Fig. 6 shows the steady-state waveforms of the converter. As shown in Fig. 6(a), the maximum and minimum voltages (v) of the resonant capacitor C_r are 35.2 V and −23.1 V, respectively, which are close to the simulated values of 34.6 V and −26.5 V, respectively. Besides, the positive and negative peak currents flowing through the switch are 13.19 A and −2.29 A, respectively, which are also close to the simulated values of 14.4 A and −2.1 A, respectively. The

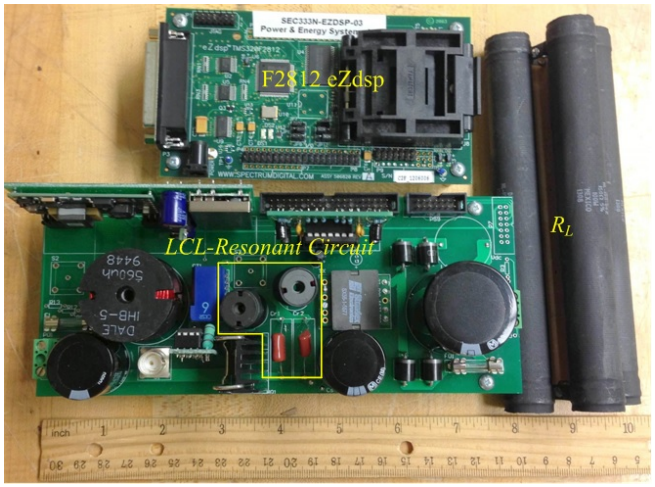

Fig. 5. The prototype of proposed converter connected to a load.

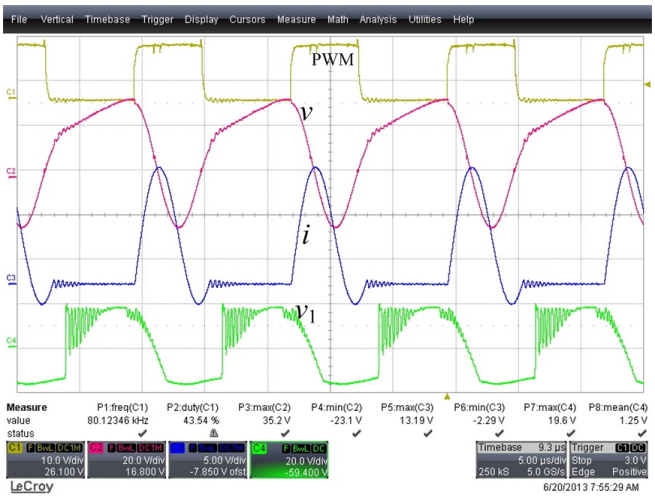

(a)

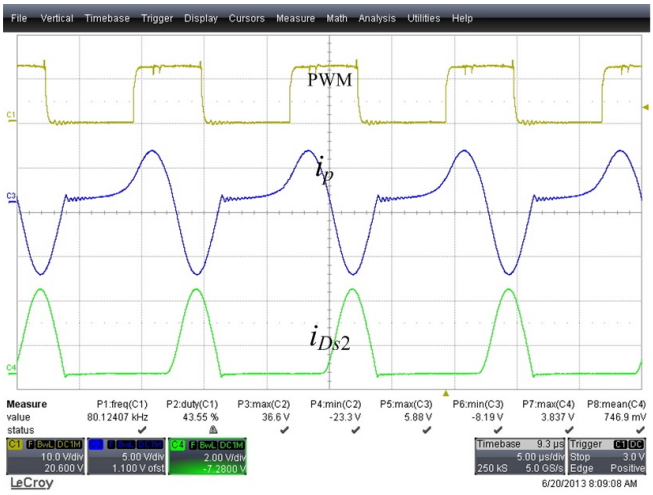

(b)

Fig. 6. The steady-state waveforms of the converter. (a) Waveforms of v, i (CH3: 1A/V) and v_1; (b) waveforms of i_p (CH3: 1A/V) and i_{Ds2} (CH4: 1A/V).

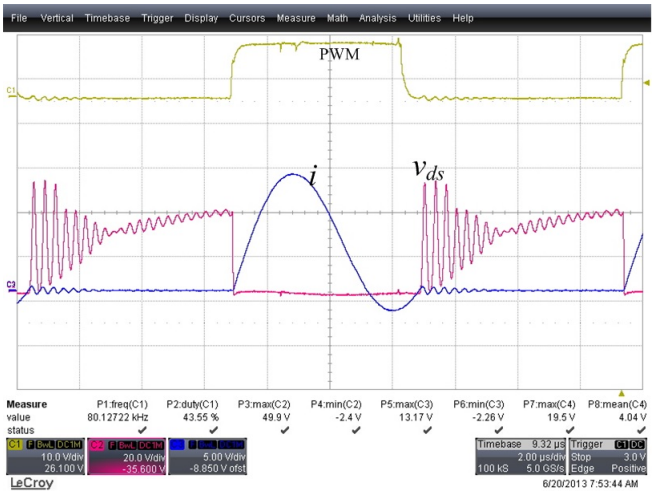

Fig. 7. The voltage and current waveforms of the switch.

waveform of v_1 also well replicates the simulation waveform. For example, the value of V_T, which equals to the maximum value of v_1, is 19.6 V in the experiment and 20 V in the simulation. Such small deviations are mainly caused by the parasitic resistance and tolerance of the components in the LCL resonant circuit. For example, the tolerances of L_r and C_r are 20% and 10%, respectively. In other words, the values of the resonant components in the experiment are not exactly the same as those used in the simulation. Fig. 6(b) shows the waveforms of the currents i_p and i_{Ds2}, which hare similar to those obtained from the simulation. D_{s2} is turned on at zero current. Thus, it is turned on under a low di/dt condition.

To testify the benefit of using the soft-switching technique, the efficiency of the proposed converter is compared to the corresponding hard-switching converter, which is obtained by removing the LCL-resonant circuit in the dash-line block of the proposed converter in Fig. 1. Fig. 8 shows compares the measured efficiencies of the converter implemented with soft-switching and hard-switching, respectively. As shown in Fig. 8, both converters has achieved over 90% efficiency when the output power is larger than 35 W. However, the proposed soft-switching converter has a higher efficiency than the hard-switching converter over the entire operating range plotted. Particularly, the soft-switching converter has achieved the maximum efficiency of 93.57% when the output power of the converter is 58 W. The increased efficiency is largely attributed to the use of the proposed soft switching technique, which has reduced the switching losses of the main switches S_1 and the rectifier diodes D_{s1}~D_{s4}.

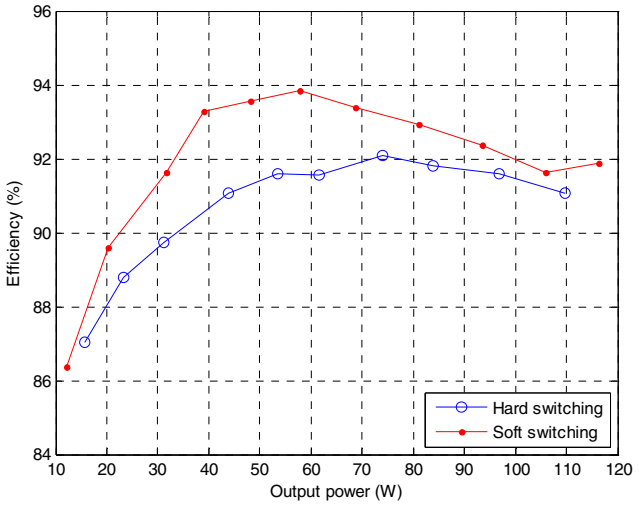

Fig. 8. Efficiency comparison between the proposed converters implemented with soft-switching and hard-switching technique.

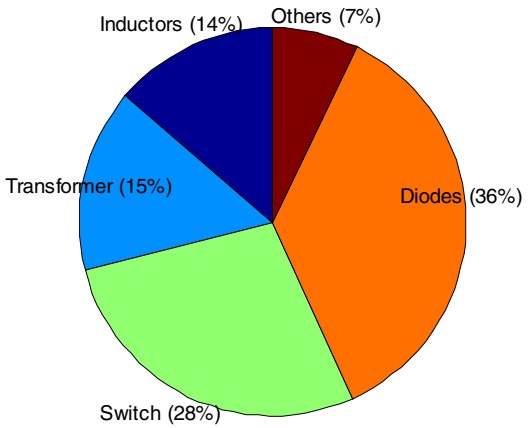

Fig. 9. Distribution of the power losses of the converter.

The distribution of power losses is analyzed among the switch, diodes, and the magnetic components, including the three inductors L_1, L_r, L_k, and the transformer. The losses of the switch and the diodes are calculated by using the measured voltage and current values with a 5 GHz sampling frequency within 200 µs. The copper losses (P_{copper}) of the magnetic components are calculated by using the measured root mean square currents and their resistances provided by the manufactures. The core losses (P_{core}) of the magnetic components are estimated as four sixths (4/6) of the corresponding copper losses, i.e., $P_{core} : P_{copper} = 4 : 6$. This is because the ratios $P_{core} : P_{copper}$ of the magnetic components were designed to be 3:7 or 4:6. Fig. 9 shows the power loss distribution when the output power is 100 W. As shown in Fig. 9, most of the losses come from the switch and the rectifier, as the percentages of the losses in the switch and in the rectifier diodes are 28% and 36%, respectively. The losses of the four magnetic components take 29% of the total loss of the converter. Therefore, a low on-resistance switch and low forward voltage diodes are preferred to further improve the efficiency of the converter.

VI. Conclusion

This paper has proposed a single-switch, LCL-resonant, isolated, DC-DC converter. The proposed converter has advantages of using the least number of switch and high efficiency. The introduced LCL-resonant circuit not only makes the switch work under soft-switching conditions, i.e., turning on under ZCS and turning off under ZVS, but also reuses the energy stored in the leakage inductance of the transformer. The proposed converter has achieved the maximum efficiency of 93.5% and has higher efficiency than the corresponding hard-switching converter over the entire operating range.

References

[1] J. Lee, B. Min, D. Yoo, R. Kim, and J. Yoo, "A new topology for PV DC/DC converter with high efficiency under wide load range," in *Proc. European Conference on Power Electronics and Applications*, Sept. 2007, pp. 1-6.

[2] C. Lohmeier, J. Zeng, W. Qiao, L. Qu, and J. Hudgins, "A current-sensorless MPPT quasi-double-boost converter for PV systems," in *Proc. Energy Conversion Congress and Exposition*, Sept. 2011, pp. 1069-1075.

[3] K. Sayed, M. Abdel-Salam, A. Ahmed, and M. Ahmed, "New high voltage gain dual-boost DC-DC converter for photovoltaic power

system," *Electric Power Components and Systems,* vol. 40, no. 7, pp. 711-728, Apr. 2012.

[4] B. Axelrod, Y. Berkovich, and A. Ioinovici, "Switched-capacitor/ switched-inductor dtructures for getting transformerless hybrid DC-DC PWM converters," *IEEE Trans. Circuits and Systems I*, vol. 55, no. 2, pp. 687-696, Mar. 2008.

[5] F. Luo, "Switched-capacitorized DC/DC converters," in *Proc. IEEE Conference on Industrial Electronics and Applications*, May 2009, pp. 1074-1079.

[6] S. Chen, T. Liang, L. Yang, and J. Chen, "A cascaded high step-up DC-DC converter with single switch for microsource applications," *IEEE Trans. Power Electronics*, vol. 26, no. 4, pp. 1146-1153, Apr. 2011.

[7] Q. Zhao and F. Lee, "High-efficiency, high step-up DC-DC converters," *IEEE Trans. Power Electronics*, vol. 18, no. 1, pp. 65-73, Jan. 2003.

[8] Y. Jang and M. Jovanovic, "Isolated boost converter," *IEEE Trans. Power Electronics*, vol. 22, no. 4, pp. 1514-1521, Jul. 2007.

[9] E. Yang, Y. Jiang, G. Hua, and F. Lee, "Isolated boost circuit for power factor correction," in *Proc. IEEE Applied Power Electronics Conference and Exposition*, Mar. 1993, pp. 196-203.

[10] H. Seong, K. Park, G. Moon, and M. Youn, "Novel dual inductor-fed DC-DC converter integrated with parallel boost converter," in *Proc. Power Electronics Specialists Conference*, Jun. 2008, pp. 2125-2131.

[11] C. Leu, P. Huang, and M. Li, "A novel dual-inductor boost converter with ripple cancellation for high-voltage-gain applications," *IEEE Trans. Industrial Electronics*, vol. 58, no. 4, pp. 1268-1273, Apr. 2011.

[12] C. Yao, X. Ruan, and X. Wang, "Isolated buck-boost DC/DC converter for PV grid-connected system," in *Proc. IEEE International Symposium on Industrial Electronics*, Jul. 2010, pp. 889-894.

[13] S. Xie and F. Li, "A novel soft switching isolated boost converter," in *Proc. IEEE Applied Power Electronics Conference and Exposition*, Mar. 2005, pp. 1375-1379.

[14] H. Krishnaswami, "Photovoltaic microinverter using single-mode isolated high-frequency link series resonant topology," in *Proc. Energy Conversion Congress and Exposition*, Sept. 2011, pp. 495-500.

[15] J. Zeng, W. Qiao, and L. Qu, "A single-switch isolated dc-dc converter for photovoltaic systems," in *Proc. IEEE Energy Conversion Congress and Exposition*, Sept. 2012, pp. 3446-3452.

[16] K. Park, C. Kim, G. Moon, and M. Youn, "New cost-effective PWM single-switch isolated converter," in *Proc. Power Electronics Specialists Conference*, Jun. 2007, pp. 1715-1720.

[17] J. Kwon, W. Choi, and B. Kwon, "Single-switch quasi-resonant converter," *IEEE Trans. Industrial Electronics*, vol. 56, no. 4, pp. 1158-1163, Apr. 2009.

[18] A. Emrani, E. Adib, and H. Farzanehfard, "Single-switch soft-switched isolated dc–dc converter," *IEEE Transactions on Power Electronics*, vol. 27, no. 4, pp. 1952-1957, April 2012.

[19] J. Zeng, W. Qiao, and L. Qu, "A soft-switching isolated multiport DC-DC converter for simultaneous power management of multiple renewable energy sources," in *Proc. IEEE Energy Conversion Congress and Exposition*, Sept. 2013, to appear.

[20] R. Steigerwald, "A comparison of half-bridge resonant converter topologies," *IEEE Trans. Power Electronics*, vol. 3, no. 2, pp. 174-182, Apr. 1988.